Research Square

Preprints are preliminary reports that have not undergone peer review.
They should not be considered conclusive, used to inform clinical practice,
or referenced by the media as validated information.

GSDME-dependent pyroptosis potentiates c-Met-targeted ADC and PD-(L)1 blockade synergy in solid tumors

Chenggang Zhao
RemeGen, Ltd
Shasha Lu
Shandong Medical and Pharmaceutical University
Jing Jiang
j_jiang@bzmc.edu.cn

Shandong Medical and Pharmaceutical University

Research Article

Keywords: antibody-drug conjugate, combination therapy, PD-1/PD-L1 blockade, pyroptosis, GSDME

Posted Date: August 3rd, 2026

DOI: https://doi.org/10.21203/rs.3.rs-10493392/v1

License: This work is licensed under a Creative Commons Attribution 4.0 International License.
Read Full License

Additional Declarations: Competing interest reported. CGZ is an employee of RemeGen, Ltd. All other authors declare no potential conflicts of interest.

Abstract

Antibody-drug conjugate (ADC) is an effective cancer therapy strategy that specifically induces tumor cell death. Combining ADC with immune checkpoint inhibitors (ICIs) has improved the clinical outcomes in some patients with solid tumors. However, the mechanism of this new combination therapy has not yet been fully elucidated. In this study, we found that monomethyl auristatin E (MMAE), a cytotoxic payload attached to RC108 (a novel c-Met-targeting ADC), activated Gasdermin E (GSDME)-induced pyroptosis in pancreatic and lung cancers. Plasma membrane rupture caused by pyroptosis releases damage associated molecular patterns (DAMPs) into the extracellular fluid, which activate immunogenic cell death (ICD) mediated by mature dendritic cell and $CD8^+$ T cells. The ICIs amplified the ICD effect together with RC108. Therefore, RC108 combined with ICIs synergistically inhibited tumor growth *in vivo*. With GSDME knocked-down, pyroptosis inhibition weakened the efficacy of the combination therapy by reducing DAMPs release. Clinically, GSDME expression was positively correlated with c-Met in patients with pancreatic cancer, indicating its benefits in RC108 combination therapy. Our findings revealed that GSDME-dependent pyroptosis improved the efficacy of the combination of ADC and ICIs, suggesting a new theoretical basis for further understanding the mechanism of such a combination strategy in solid tumor treatment.

Background

Antibody drug conjugate (ADC), known as " biological missile" in the field of anti-tumor therapy, is constantly being explored(1–4). Currently, there are more than 10 ADCs are approved for global listing(2, 5, 6). ADC means that monoclonal antibody is covalently linked to cytotoxic drugs via a chemical linker and selectively delivers highly effective cellular agents to target cancer cells by targeting cell surface markers(3). With the differential expression of targets between tumor and normal cells, ADC can enhance efficacy and limit toxicity(3). However, owing to the complex pathogenesis of tumors and the positive correlation between the efficacy of ADC alone and the target level, only a small number of cancer patients benefit from long-term treatment(7). Immunotherapy for cancer is another hot research field in which overcoming immunosuppression is the central mechanism(8, 9). Immune checkpoint inhibitors (ICIs), which block the signaling of programmed cell death protein 1 (PD-1) and programmed cell death 1 ligand 1 (PD-L1), have been widely used in clinical practice(10–12). In fact, ICIs demonstrate a good clinical outcome only in a few malignancies, such as melanoma, non-small cell lung cancer, and renal cell carcinoma, indicating that blocking inhibitory signals is not sufficient for patients without sufficient anti-tumor immune capability(11, 13, 14). Therefore, it is necessary to combine other therapies to increase drug sensitivity and expand the beneficial population.

Combining ADC with ICIs is a promising therapeutic strategy(15). Multiple biological mechanisms have been reported to support the rationality of this design(16–19). Among these, immunogenic cell death (ICD) caused by small molecular toxins conjugated to ADC is the most significant mechanism(20). ICD involves endoplasmic reticulum stress (ER-Stress) and the release of damage-related molecular patterns (DAMPs) from dying tumor cells, including Calreticulin (CRT), ATP, high mobility group box 1 (HMGB1),

heat shock protein 70 (HSP70) and heat shock protein 90 (HSP90)(21). The activation of these DAMPs molecular signals promotes dendritic cell (DC) migration to tumor tissue and DC maturation, thereby altering antigen presentation and increasing T-cell infiltration into the tumor microenvironment(21–23). ICIs rejuvenate exhausted T cells and enhance antitumor immune responses(13). Therefore, ADC can act synergistically with ICIs to exert therapeutic effects(16).

Pyroptosis, also known as cell inflammatory necrosis, depends on the activation of caspases and cleavage of gasdermin (24, 25). The released N-terminal of Gasdermin-E (GSDME) binds to membrane lipids and perforates the cell membrane, resulting in changes in cell osmotic pressure, cell swelling, and membrane rupture(24). Recent studies have shown that classic tumor pyroptosis signals are mediated by gasdermin-D (GSDMD). Pathogens, such as bacteria and viruses, activate Csapase1 by stimulating cells to form inflammasome protein complexes. Activated Csapase1 cleaves GSDMD, interleukin-1β and interleukin-18, respectively, amplifying the inflammatory response by inducing GSDMD-dependent pyroptosis(25, 26). However, chemotherapy drugs and radiotherapy transform apoptosis into pyroptosis in tumor cells expressing GSDME by activating Caspase3. Similar to the Caspase1-GSDMD axis, Caspase3 directly cleaves GSDME to localize its N-terminus to the membrane(27, 28). Pyroptosis is also a crucial natural immune response. Under the conditions of GSDME activation, the ICD effect is activated by DAMPs release(24). Additionally, it was recently discovered that granzyme B (GzmB) secreted by natural killer (NK) and $CD8^+$ T lymphocytes can directly cleave the D270 site of GSDME to activate pyroptosis. This finding highlights the importance of GSDME-mediated pyroptosis in anti-tumor immunotherapy through the interaction between tumor cells and immune cells(29).

Here, we found that RC108, a novel ADC targeting c-Met, induces GSDME-dependent pyroptosis in pancreatic and lung cancers. Pyroptosis enhanced DAMPs release promoted DC maturation and ICD effect. Therefore, pyroptosis is conducive to the synergistic effects of the combination of drugs.

Materials and methods

Antibodies and reagents

Antibodies against GSDME (84005), cleaved-GSDME (55879), GSDMD (39754), GAPDH (92310), Caspase3 (9662), cleaved-Caspase3 (9664), C/EBP homologous protein (CHOP) (2895), Phospho-SAPK/c-Jun N-terminal kinase (JNK) (4668), Phospho-eIF2α (3398), and protein-kinase-like ER kinase (PERK) (3192) were purchased from Cell Signaling Technology (CST). Anti-IRE1 (phosphor-S724) (ab48187) and Anti-IRE1 (ab37073) were purchased from Abcam. AlexaFluor488 goat anti-rabbit IgG (A11034) and AlexaFluor568 goat anti-rabbit IgG (A11036) were purchased from Invitrogen (Carlsbad, CA). Hochest (62249) was purchased from Thermo Fisher Scientific.

RC108 (RC108-ADC), monomethyl auristatin E (MMAE), RC108-0 (uncoupled MMAE), hIgG-ADC, and RC98 were obtained from RemeGen, Ltd. Opdivo (ABX8463) was from Bristol Myers Squibb (BMS). AC-

DEVD-CMK was purchased from MedChemExpress (Shanghai, China). DMSO (D2650) was purchased from Sigma-Aldrich. Matrigel (354234) was from Corning (Corning, NY).

Cell culture

All cell lines used in this study were obtained from the ATCC. HPAC, NCI-H226, MDA-MB-231, and CAKI1 cell lines were cultured respectively in DMEM/F12, RPMI1640, DMEM, and McCOY's5A (meilunbio, China) containing 10% fetal bovine serum (HyClone, USA) and 1% Penicillin-Streptomycin Solution (Spark Jade, China). The cell lines were regularly confirmed to be Mycoplasma free.

RC108 lysosomal transport assay

RC108-ADC, hIgG-ADC, and RC108-0 were directly labeled with green fluorescence by Alexa Fluor488 Monoclonal Antibody Labeling Kit (A20181, Thermo Fisher scientific). The fluorescent markers were incubated with MKN-45 and CAKI1 cells at 4 ℃ for 30 min and 37 ℃ for 16 hours respectively. Lyso Tracker Red DND-99 (L7528, Thermo Fisher scientific) was used to label lysosomes, and DAPI (C1005, Beyotime, China) was used to stain nucleus. The EVOS™ FL Auto2 imaging system was for capturing.

Flow cytometry analysis

To detect c-Met expression in the cell lines, the QIFIKIT (Dako) indirect immunofluorescence method was used to measure the antigen density on the cell surface. 5×10^5 cells were incubated with c-Met antibody (MAB3582, R&D Systems) and FITC-Conjugated anti-mouse antibody (F0103B, R&D Systems) at 4 ℃ for 1h successively. The QIFIKIT SET-UP BEADS and CALIBRATION BEADS (K0078, Dako) were used to follow the instructions for subsequent operations. The flow cytometer (SA3800, SONY) was used for analysis of cells and BEADS samples. The fluorescence values of the cell samples were substituted into the standard curve to obtain antigen expression values.

For immune cell profiling, all cell markers were sourced from BioLegend (USA). The tumor tissues were cut into small pieces of 3-5mm and digested at 37°C with 200U/mL collagenase IV for 30 minutes. The digested product was filtered using a 100μm cell filter to obtain a single-cell suspension. The suspension was resuspended in diluted Zombie (77477) dye in the dark for 15–30 min. The Fc receptor blocking step was necessary for staining DC cells. Mouse TruStain FcX ™ PLUS (156604) was used to bind the FC receptors on the DC surfaces. Next, the cell pellet was stained with hCD45-Pacific Blue (304029), hCD8-FITC (301006), mCD11c-PerCP/Cyanine5.5 (117328) and mMHCII-APC/Cyanine7 (107628) for 30 min at 4 ℃ and analyzed at flow cytometer (SA3800, SONY).

Immunoblotting

The cell pellet for protein expression detection was lysed by RIPA buffer (Beyotime, China) containing a cocktail protease inhibitor (Roche). The BCA method was used for quantitative analysis of the lysate. According to the quantitative results, all the groups were unified at the same concentration. The lysate was then boiled at 95 ℃ for 10 min. For SDS-PAGE, gradient gels (M00657, GenScript, China) with a concentration range of 4–20% were used to separate protein samples. The separated proteins were transferred onto a nitrocellulose membrane. The membrane was blocked with 5% milk in PBST at room temperature for 1h. The corresponding primary antibody was used to incubate the blocked membrane overnight at 4 ℃. After combining with secondary antibodies from the same species, protein bands were visualized by chemiluminescent substrates (34095, Thermo Fisher scientific).

Cell proliferation assay and cell apoptosis assay

The Cell Counting Kit-8 (C0040, Beyotime, Shanghai, China) was used to detect cell viability. In a 96-well plate, 4000 cells were inoculated into each well and repeated for 5 wells per group. The read OD value was calculated as the inhibition rate, and the inhibition rate formula was: IR% = ($OD_{blank} - OD_{drug}$) × 100/OD_{blank}. GraphPad Prism 8.0 was used to calculate the concentration of the drug with 50% inhibition rate (IC50 calculation formula: 50 = Bottom+(Top-Bottom)/(1 + 10^(LogIC50-x) × Hillslope), IC50 = 10^ X).

Cell counting was performed to assess cell proliferation. Cells (2×10^5) were inoculated into each culture in a 12-well plate. After treatment with different concentrations of RC108, the cells with GSDME knockdown were digested and resuspended for counting.

Cell apoptosis assays were performed using a FITC Annexin V Apoptosis Detection Kit with PI (AD10/PS541, DojinDo, Japan) following the manufacturer's instructions for experimental procedures.

siRNA transfection

All siRNAs were synthesized by Sangon Biotech (Shanghai, China). The siRNA sequences were as follows. GSDME siRNA-1, GCAUUCAUAGACAUGCCAGAUTTAUCUGGCAUGUCUAUGAAUGCTT. GSDME siRNA-2, GAUGAUGGAGUAUCUGAUCUUTTAAGAUCAGAUACUCCAUCAUCTT. siRNAs were transfected into cells for 48h using Lipofectamine 3000 (L3000015, Invitrogen) according to the manufacturer's instructions.

LDH and DAMPs release detection

HPAC cells were seeded at 250,000 cells per well and incubated in a 6-well plate at 37 ℃ for 16 h. On the second day, PBS, RC108 or MMAE at the concentrations shown in the figure were added to the wells and incubated at 37 ℃ for 48 h. The supernatant was added to 96 well plates for the detection of LDH and DAMPs contents. LDH was detected using the CytoTox 96 NonRadio (G1781, Promega) assay kit,

ATP was detected using the CellCounting Lite 2.0 (DD1101, Vazyme, Nanjing, China) assay kit, and HMGB1 (R&D Systems), HSP70 (R&D Systems), and HSP90 (Elabscience) were evaluated using specific ELISA kits according to standard procedures.

For cell supernatant detection following GSDME knockdown, HPAC cells were treated with RC108 (500ng/mL) for 48 h after RNAi manipulation for 24 h.

Peripheral blood mononuclear cell (PBMC) killing assay

PBMCs used in this study were from Oribiotech (Shanghai, China). First, HPAC cells were seeded at 3,000 cells per well and incubated in a 96-well plate at 37 ℃ for 16 h. Subsequently, siRNA was added to the cell supernatant according to the instructions of Lipofectamine 3000. After 24 h, 5×10^4 PBMC cells in 50μL/well were added to the plate with HPAC cells. The treatment groups including PBS group, RC108 group, Opdivo group, and RC108 + Opdivo groups, were added to the corresponding wells containing target cells and effector cells at 37 ℃ for 72 h. Removing the effect cells in the supernatant, the viability of tumor cells was detected by Cell Counting Kit-8 (C0040, Beyotime, Shanghai, China).

Cytokine detection

At the endpoint of the mouse study (Day24), the serum from all groups was collected. After centrifugation at 3,500 rpm for 15 min at 4 ℃, the levels of IL-1β, IL-6, IL-12, TNF-α, and IL-18 in mouse serum were detected by standard Cytometric Bead Array (CBA) procedures using commercially available kits (BioGend). Serum levels of Granzyme B were evaluated using a specific ELISA kit (R&D Systems) according to the manufacturer's instructions.

Immunofluorescence and immunohistochemistry

Cells were inoculated in a 96-well plate protected from light. Immunofluorescence was performed at a cell density of 60%. The cells were fixed with 4% paraformaldehyde and incubated with the antibodies shown in the figure. The cells were imaged using an inverted microscope (EVOS FL AUTO 2, Invitrogen).

For immunohistochemical staining of the pancreatic cancer tissue chip (OUTDO BIOTECH, Shanghai, China), a series of xylene deparaffinization and alcohol rehydration steps followed by antigen retrieval (10 mM sodium citrate) were used. Antibodies against GSDME (PA5-109333) and c-Met (8198) were purchased from Invitrogen and CST, respectively. To quantify the expression of GSDME and c-Met, IHC staining was quantified using scores of 0 (0%), 1 (0–20%), 2 (20–40%), 3 (40–60%), 4 (60–80%), and 5 (80–100%).

Immune reconstitution and xenograft studies

All *in vivo* combination therapy experiments were performed on B-NDG female mice aged 7 weeks (Biocytogen, China), and 3–4 mice are housed in a cage. The animal experiment was approved by the Institutional Animal Care and Use Committee (IACUC) of Remegen, Ltd, and conducted in accordance with the Institutional Animal Care and Use Guidelines. The operators were not aware of the specific

situation of each group's medication. Each operation and measurement were carried out in a uniform order. Mice were inoculated subcutaneously into the right flank with 3×10^6 HPAC cells in 1:1 Matrigel (Corning) and DMEM/F12 medium. When the tumor volume reached 120-200mm^3, the mice bearing tumors were injected with human PBMC through tail vein injection, which was labeled as Day-1. Tumor-bearing mice with tumor volumes outside the range of 120-200mm^3 will be eliminated. Tumor-bearing mice were randomly allocated to each group following the principle of homogeneous tumor volume distribution to ensure comparable baseline tumor volumes across all experimental groups. On Day 0, vehicle (PBS), RC108-ADC (3mg/kg), RC98 (10mg/kg), Opdivo (10mg/kg), RC98 + RC108-ADC (10mg/kg+3mg/kg), and Opdivo+RC108-ADC (10mg/kg+3mg/kg) were administered respectively (n = 10). Except for RC108, which was administered only once, all other groups were administered twice per week. During the experiment, tumor volume and body weight were measured twice per week. On the 24th day of administration, the study was terminated. 200–400μL of peripheral blood were collected from each group of experimental animals for cytokine analysis. All mice were euthanized, photographed, and then dissected as soon as possible to obtain tumor tissue. After the tumors were weighed, half of them were extracted with protein for the Western blot assay, and the rest were analyzed by flow cytometry for tumor infiltrating lymphocyte. No mice were excluded from each group in the above experiments. EXCEL software was used to calculate the tumor volume, tumor weight, Tumor Growth Inhibition (TGI), body weight change rate (BWC), and combined drug effect index (Q).

The calculation formula was as follows: $TGI\%=(C_{TW}-T_{TW})/C_{TW}\times100\%$; $C_{TW,}$ means tumor weight in the control group; and $T_{TW,}$ means tumor weight in the treatment group. $Q = P(O)/(P(A) + P(B)-P(A)\times P(B))$; P(O), TGI for drug combination; P(A), TGI for drug A; P(B), TGI for drug B.

Bioinformatics and statistical analyses

Gene expression data from The Cancer Genome Atlas (TCGA) was obtained and analyzed using TIMER2.0 (http://timer.comp-genomics.org/) and Gene Expression Profiling Interactive Analysis (GEPIA2).

Multiple group comparisons were performed using one-way analysis of variance (ANOVA). The two-tailed t-test was used to assess the statistical differences between the two groups. For the correlation analysis between GSDME and $CD8^+$ T cell infiltration, the significance of the differences among the indicated groups was determined using the χ^2 test. The Pearson's correlation test was used to analyze the correlation between GSDME expression and c-Met levels in the tissues. All statistical analyses are shown as mean ± SD. The number of repetitions for each experiment is presented in the legend. Statistical significance was set at $P < 0.05$.

Results

RC108 and MMAE induce pyroptosis in pancreatic cancer and lung cancer

First, we characterized the biological activity of RC108. RC108 bound to c-Met on the cell surface with high activity and was internalized into the lysosomes within 16 h (Fig. 1A; Supplementary Fig. S1A-B). Next, we detected the expression of c-Met protein in existing cell lines in our laboratory, and RC108 treatment was applied to the cell lines with high c-Met expression (Fig. 1B). It was found that obvious pyroptosis phenotype occurred in HPAC, NCI-H226, MDA-MB-231 and CAKI1 cells (data for the latter two cell lines not shown) (Fig. 1C; Supplementary Fig. S1C). At lower IC50 values, RC108 effectively inhibited the growth of tumor cell lines (Fig. 1D; Supplementary Fig. S1D-E). Over time, RC108 and MMAE induced cell death, as detected by Annexin-V and Propidium Iodide (PI) staining assay (Fig. 1E-F). LDH release was also increased by RC108 or MMAE treatment, suggesting the occurrence of pyroptosis (Fig. 1G).

Caspase3-GSDME axis is the executor of pyroptosis induced by RC108

As chemotherapy drugs often induce pyroptosis through GSDME(27), we tested GSDME expression in various cell lines. It was found that pancreatic cancer cell HPAC and lung cancer cell NCI-H226 expressed the highest levels of GSDME (Fig. 2A). Increasing concentrations of RC108 and MMAE induced cleavage of the N-terminus of GSDME (but not GSDMD) in both cell lines, mediated by Caspase3 (Fig. 2B-C; Supplementary Fig. S2A). Immunofluorescence assay also showed that RC108 induced cleaved-GSDME membrane localization in NCI-H226 cells, which directly reflected that MMAE-induced pyroptosis was activated by GSDME (Fig. 2D). To evaluate the role of Caspase3 signal, Ac-DEVD-CMK, a Caspase3 inhibitor, was used to treat the tumor cells. As shown in the figure, the inhibitor reversed GSDME activation by RC108, which was validated in both cell lines (Fig. 2E-F). Pyroptosis induced by RC108 was also weakened with Caspase3 inhibited (Supplementary Fig. S2B). Taken together, these data suggest that RC108 and MMAE activated pyroptosis mediated by the Caspase3-GSDME axis in pancreatic and lung cancer cells.

Pyroptosis contributes to the anti-tumor effects of RC108 in combination with PD-1 blockade, inhibiting tumor cell growth in vitro.

To evaluate the effect of pyroptosis on the cytotoxicity of RC108, GSDME protein was knocked down using RNA interference technology. In HPAC and NCI-H226 cells, reduced GSDME only weakly inhibited the efficacy of RC108 at low concentrations (Fig. 3A-C).

Pyroptosis is regarded as an inflammatory death mode that activates the immune microenvironment and helps convert “cold” tumors into “hot” tumors(30). To evaluate the correlation between pyroptosis and anti-tumor immunity, we analyzed pancreatic cancer data from The Cancer Genome Atlas (TCGA) in TIMER2.0 website. The analysis results showed that GSDME was positively correlated with the infiltration of $CD8^+$ T cells and NK cells in patients with pancreatic cancer (Fig. 3D). Immunotherapy based on blocking PD-1/PD-L1 signals with ICIs is gradually being applied in clinical practice(11). We wondered whether pyroptosis could regulate the combination of ADC and ICIs in tumor treatment. Therefore, we simulated the anti-tumor immune response induced by ADC and ICIs *in vivo* by co-culturing

PBMC and HPAC cells *in vitro*. Subsequently, the mixed cells were treated with PBS, RC108, Opdivo (a PD-1 monoclonal antibody), and RC108 combined with Opdivo. It was found that the cytotoxicity of the RC108-Opdivo combination group was stronger than that of the monotherapies (Fig. 3E). As GSDME decreased, the killing ability of PBMC in the RC108 alone and combination groups was significantly weakened, indicating that pyroptosis upregulated PBMC activity (Fig. 3E).

RC108 and MMAE activate pyroptosis-mediated DAMPs release

Next, we investigated the effect of pyroptosis on ADC in combination with Opdivo. Both RC108 and MMAE induced DAMPs activation. Following drug treatment, intracellular CRT expression increased. Similarly, ATP, HMGB1, HSP70, and HSP90 secretion in the culture supernatant of HPAC cells was also elevated (Fig. 4A-E). In addition, the intracellular levels of HSP70 and HSP90 were significantly increased by RC108 and MMAE (Supplementary Fig. S3A-B). Augmenting these DAMPs signals aids in the recruitment of DC to target tumors and promotes antigen presentation(21). However, the levels of ATP, HMGB1, HSP70 and LDH in the culture supernatant decreased upon GSDME knock down (Fig. 4F-I). These results indicated that GSDME-mediated pyroptosis contributed to the extracellular release of DAMPs, thereby modifying the tumor microenvironment.

RC108 combined with PD-1/PD-L1 mAb exerts synergistic tumor inhibition effect

To clarify the role of pyroptosis in the combination strategy, we established an immune reconstituted subcutaneous transplant tumor model with HPAC cells based on human PBMC in immunodeficient mice (Fig. 5A). After 14 days, we discovered that the combination of Opdivo or RC98, a PD-L1 inhibitor provided by RemeGen, Ltd, yielded remarkable improvements in the anti-tumor effect of RC108 in terms of tumor volume and weight compared to the individual treatments (Fig. 5B-C; Supplementary Fig. S4A-C). The combination regimens generated synergistic anti-tumor effects at the experimental endpoint (Q = 1.22) (Fig. 5A). Remarkably, there was no noticeable weight loss in any of the groups, indicating that the drugs were well-tolerated (Fig. 5D).

We then studied protein expression in the tumor tissue and observed the activation of ER-stress signals, such as PERK, eukaryotic initiation factor-2alpha (eIF2α), inositol-requiring enzyme 1 (IRE1), and JNK, especially in the combination groups. Furthermore, CHOP, a transcription factor linked to a switch from survival to apoptosis in the ER-stress pathway(31), was activated in the combination groups, suggesting the onset of cell death (Fig. 5E).

RC108 alone or in combination with ICIs induces tumor pyroptosis and immunogenic cell death

In the tumor extract from RC108 monotherapy or combined with RC98/Opdivo, Caspase3 and GSDME (instead of GSDMD) were consistently activated. Compared with RC108 alone, the expression of GSDME-

NT was found to be higher in the combined group, while cleared Caspase3 was not (Fig. 6A). The above data proved that the combined strategy induced more pyroptosis. Flow cytometry results showed that the infiltration of $CD45^+$ leukocytes and DC into the tumor in the combination group was significantly increased, and $CD8^+$ T cells also showed an upward trend in each treatment group (Fig. 6B-D). Among inflammatory cytokines, IL-1β, IL-6 and IL-12 are mostly released by mature DCs(20, 32). TNF-α and IL-18 are two other important pro-inflammatory and anti-tumor protein(33, 34). In the serum, the levels of IL-1β, IL-6, IL-12, TNF-α, and IL-18 were increased to some extent, indicating enhanced antigen presentation and a boosted immune response (Fig. 6E-I).

Furthermore, the GzmB level was significantly increased in the RC98 and combination groups (Fig. 6J). GzmB facilitates the direct cleavage of GSDME to induce pyroptosis(29), providing a possible explanation for the higher expression of GSDME-NT in the combination group (Fig. 6A). These results suggest that ICD was the key factor for the synergistic anti-tumor effect of RC108 combined with ICIs *in vivo*, which was amplified by pyroptosis.

GSDME is a suitable screening marker for the combination therapy of ADC targeting c-Met and PD-1/PD-L1 blockade in pancreatic cancer

In this section, we focus on the clinical applications of pyroptosis. Through analyzing clinical sample data obtained from The Cancer Genome Atlas (TCGA), we found a positive correlation between the expression of GSDME and the RC108 target c-Met in pancreatic cancer patients (Fig. 7A). The above findings were confirmed by immunohistochemical staining of 71 pancreatic cancer tissue samples (Fig. 7B). Quantification of staining on a scale of 0 to 5 points showed that the correlation was significant (Fig. 7C). Since the efficacy of ADC is usually related to the target level, GSDME-mediated pyroptosis could be particularly helpful in improving the efficacy of RC108 in pancreatic cancer. Compared to tumor infiltrating lymphocyte (TIL) information obtained from the tissue microarray, we also found a significant correlation between GSDME expression and the infiltration of $CD8^+$ T cells in pancreatic cancer tissue samples (Supplementary Table S1). In summary, these results further revealed that the activity of GSDME was positively associated with the TIL of human pancreatic cancer, which was beneficial in improving the efficacy of RC108 combined with ICIs.

Discussion

Although the treatment regimen of ADC combined with ICIs is undergoing extensive clinical trials, the mechanism still requires further research. Our study revealed that pyroptosis enhanced the efficacy of combination therapy. First, the cytotoxic payload MMAE coupled to ADC induced pyroptosis in pancreatic cancer and lung cancer models. Second, pyroptosis could cause an inflammatory reaction and induce DC and cytotoxic T cells to penetrate the tumor microenvironment (Fig. 7D). Finally, the expression of GSDME and c-Met in pancreatic cancer patients was positively correlated, indicating the potential therapeutic benefits of combination therapy for pancreatic cancer patients with high expression of c-Met.

The mechanism of ADC induced ICD has been confirmed in several studies. Based on this principle, multiple preclinical studies have been reported on the combination of ADC and ICIs(16). Enapotamab vedotin (EnaV), an antibody-drug conjugate targeting AXL receptor tyrosine kinase, induced inflammation and ICD in tumor cells and promoted the induction of memory-like phenotypes in cytotoxic T cells. In melanoma and lung cancer models, the combination of EnaV and tumor specific T cells was superior to the single treatment(17). Brentuximab vedotin (BV) was an antibody-drug conjugate targeting CD30. BV could induce DC homing and activate anti-tumor immune response. A substantial synergistic therapeutic effect was observed when BV was combined with tumor antigen-specific vaccines or the PD-1-PD-L1 and CTLA-4 co-inhibitory pathways(19, 20). Disitamab vedotin (RC48) was defined as a HER2 directed antibody-drug conjugate. The combination of RC48 and anti-PD-1/PD-L1 significantly enhanced tumor suppression and anti-tumor immunity. The tumor rejection response in the synergistic group was accompanied by a large amount of T cell infiltration and activation of immune markers(18). Trastuzumab deruxtecan (DS-8201a) was another antibody-drug conjugate targeting HER2. DS-8201a upregulated tumor infiltrating DC and $CD8^+$ T cells *in vivo*, and enhanced the expression of PD-L1 and MHC class I in tumor cells. These cases provided a powerful reference for our projection(35).

Since the physiological mechanism of pyroptosis has been elucidated, its role in the field of anti-tumor immunity has gradually been elucidated as well. One notable feature that distinguishes pyroptosis from other cell death modes is that it can cause a strong inflammatory response, including the LDH and DAMPs release and ICD(36, 37). Studies have shown that chemotherapy-induced pyroptosis is often mediated by activated GSDME(27). Our results showed that the small molecule toxin MMAE induced pyroptosis by activating Caspase3 and subsequent cleavage of GSDME-NT. Caspase3 is a key executor of cell death, switching cell fate between apoptosis and pyroptosis, which often depends on the expression level of GSDME(28). However, unlike Wittner et al.'s report that inhibiting pyroptosis reversed the efficacy of ADC (38), we did not detect a significant change in the cytotoxicity of ADC when GSDME was silenced at the cellular level, although their study also found that pyroptosis induced by microtubule inhibitors activated ICD.

The collaboration between ADC, pyroptosis, and immunotherapy is not the first time in the field of cancer treatment. Wang et al. delivered GSDMA3 protein to 4T1 tumor cells based on a bioorthogonal system, making tumor tissue sensitive to PD-1 therapy by activating the immune response. Tumor regression does not exist in immunodeficient mice or in T cell depletion(39). Our experiment was based on a mouse model of human PBMC immune reconstitution. The results showed that when GSDME was silenced, the ability of RC108 to induce DAMPs in HPAC cells was weakened. In animal models, RC108 successfully activated DC and $CD8^+$ T cells.

Consistent with Caspase3, GzmB is recently found to directly cleave the Asp270 site of GSDME. Our results showed that the combination group had higher levels of GzmB(29). Positive feedback regulation based on pyroptosis reflected the interaction between tumor cells and effector cells. The mechanism of GzmB in the ADC-pyroptosis-ICIs axis still needs to be further demonstrated by altering GzmB expression.

Pancreatic cancer is one of the most aggressive and chemoresistant cancer types. The clinical efficacy of immunotherapy is also limited in pancreatic cancer, mainly because of the complexity of the immunosuppressive tumor microenvironment(40). Wang et al. used a membrane-targeted photosensitizer TBD-3C with aggregation-induced emission characteristics to trigger pyroptosis-induced cancer immunotherapy. The new method not only inhibited the growth of primary pancreatic cancer, but also attacked distant tumors(37). Our research was also based on a pancreatic cancer model and found that the expression of GSDME was positively correlated with the level of RC108 target c-Met and tumor-infiltrating lymphocytes, which highlighted the research value of pyroptosis in pancreatic cancer. Among candidates with pancreatic cancer undergoing RC108 treatment, GSDME has the potential to become a molecular marker for determining whether it is suitable for treatment with ICIs.

In summary, we have demonstrated a new mechanism of ADC combined with ICIs for the treatment of solid tumors. The payload MMAE on the ADC targeting c-Met activates the tumor microenvironment by inducing pyroptosis, which sensitizes ICIs. Our data provides a strong theoretical basis for clinical research on the combination of RC108 and immunotherapy. In addition, the expression characteristics of GSDME provide a new insight for the combination therapy in pancreatic cancer.

Declarations

Acknowledgments

We thank the members of the Non-Clinical Research Department, RemeGen, Ltd.

Declaration of interest statement

CGZ is an employee of RemeGen, Ltd. All other authors declare no potential conflicts of interest.

Data availability statement

All data generated or analyzed during this study are included within this article or upon request from the corresponding author.

Funding

This research was supported by the Shandong Provincial Natural Science Foundation (NO. ZR2024QH648); Shandong Provincial Postdoctoral Foundation Project (Innovation Project), (NO. SDCX-ZG-202301018).

Contributions

JJ and CGZ conceived and designed the experiments; CGZ and SSL performed the experiments; CGZ, and JJ analyzed the data; CGZ wrote the paper; CGZ and JJ revised the manuscript. All authors have read and approved the final manuscript.

Ethics approval and consent to participate

The animal experiment was approved by the Institutional Animal Care and Use Committee (IACUC) (ID: AUP-S-2022-038-M-01-001) of Remegen, Ltd, and conducted in accordance with the Institutional Animal Care and Use Guidelines. The PBMCs used in this study were obtained from Oribiotech (Shanghai, China) following written informed consent. Our study adheres to the declaration of Helsinki.

Consent for publication

Not applicable.

References

1. Géraud A, Gougis P, de Nonneville A, Beaufils M, Bertucci F, Billon E et al (2025) Pharmacology and pharmacokinetics of antibody-drug conjugates, where do we stand? Cancer Treat Rev 135:102922
2. Fu Z, Li S, Han S, Shi C, Zhang Y (2022) Antibody drug conjugate:thebiological missilefor targeted cancer therapy. Signal Transduct Target Therapy. (004):007
3. Tsuchikama K, An Z (2016) Antibody-drug conjugates: recent advances in conjugation and linker chemistries
4. Chau C, Steeg P, Figg W (2019) Antibody-drug conjugates for cancer. Lancet (London England) 394(10200):793–804
5. Tarantino P, Pestana RC, Corti C, Modi S, Bardia A, Tolaney SM et al (2022) Antibody-drug conjugates: Smart chemotherapy delivery across tumor histologies. Cancer J Clin
6. Li N, Yang L, Zhao Z, Du T, Liang G, Li N et al (2025) Antibody-drug conjugates in breast cancer: current evidence and future directions. Experimental Hematol Oncol 14(1):41
7. Drago JZ, Modi S, Chandarlapaty S (2021) Unlocking the potential of antibody-drug conjugates for cancer therapy. Nat reviews Clin Oncol
8. O'Donnell JS, Teng M, Smyth MJ Cancer immunoediting and resistance to T cell-based immunotherapy. Annals Am Thorac Soc. 2019(3):16
9. Makkouk A, Weiner GJ (2015) Cancer Immunotherapy and Breaking Immune Tolerance: New Approaches to an Old Challenge. The official organ of the American Association for Cancer Research, Inc., Cancer research
10. Li HY, Mcsharry M, Bullock B, Nguyen TT, Kwak J (2017) The Tumor Microenvironment Regulates Sensitivity of Murine Lung Tumors to PD-1/PD-L1 Antibody Blockade. Cancer Immunol Res 5(9):767–777
11. Bagchi S, Yuan R, Engleman EG (2021) Immune Checkpoint Inhibitors for the Treatment of Cancer: Clinical Impact and Mechanisms of Response and Resistance. Annual Rev Pathol Mech Disease. ;16(1)

12. Budimir N, Thomas GD, Dolina JS, Salek-Ardakani S (2022) Reversing T-cell Exhaustion in Cancer: Lessons Learned from PD-1/PD-L1 Immune Checkpoint Blockade. Cancer Immunol Res 10(2):146–153
13. Hussaini S, RaniaBoldt R, GabrielRaphael (2021) JacquesBlanchette, PhillipVareki, Saman MalekiFernandes, Ricardo. Association between immune-related side effects and efficacy and benefit of immune checkpoint inhibitors-A systematic review and meta-analysis. Cancer Treat Rev. ;92(1)
14. Hagiwara M, Fushimi A, Matsumoto K, Oya M (2022) The Significance of PARP1 as a biomarker for Predicting the Response to PD-L1 Blockade in Patients with PBRM1-mutated Clear Cell Renal Cell Carcinoma. Eur Urol 81(2):145–148
15. Fuentes-Antras J, Genta S, Vijenthira A, Siu LL (2023) Antibody-drug conjugates: in search of partners of choice. Trends Cancer 9(4):339–354
16. Ena B, Fga B, Laa B, Ptabc D, Cca B, Smtc D et al (2022) Combining Antibody-drug Conjugates with Immunotherapy in Solid Tumors: Current Landscape and Future Perspectives. Cancer Treat Rev 106:102395
17. Boshuizen J, Pencheva N, Krijgsman O, Altimari DD, Peeper DS Cooperative Targeting of Immunotherapy-Resistant Melanoma and Lung Cancer by an AXL-Targeting Antibody-Drug Conjugate and Immune Checkpoint Blockade. Cancer Res. 81(7):1775–1787
18. Huang L, Wang R, Xie K, Zhang J, Tao F, Pi C et al (2022) A HER2 target antibody drug conjugate combined with anti-PD-(L)1 treatment eliminates hHER2 + tumors in hPD-1 transgenic mouse model and contributes immune memory formation. Breast Cancer Res Treat. (1):191
19. Cao AT, Law CL, Gardai SJ, Heiser RA (2017) Abstract 5588: Brentuximab vedotin-driven immunogenic cell death enhances antitumor immune responses, and is potentiated by PD1 inhibition in vivo. Cancer Res 77(13 Supplement):5588
20. Müller P, Martin K, Theurich S, Schreiner J, Savic S, Terszowski G et al Microtubule-Depolymerizing Agents Used in Antibody–Drug Conjugates Induce Antitumor Immunity by Stimulation of Dendritic Cells. J Immunother Cancer. 2014(8).
21. Krysko DV, Garg AD, Kaczmarek A et al (2012) Immunogenic cell death and DAMPs in cancer therapy. Nat Rev Cancer
22. Bian Z, Shi L, Kidder K, Zen K, Liu Y (2021) Intratumoral SIRPα-deficient macrophages activate tumor antigen-specific cytotoxic T cells under radiotherapy. Nat Commun 12(1):3229
23. Steinman RM (1991) The dendritic cell system and its role in immunogenicity. Annu Rev Immunol 9(1):271–296
24. Shi J, Gao W, Shao F (2017) Pyroptosis: Gasdermin-Mediated Programmed Necrotic Cell Death. Trends Biochem Sci
25. Shi J, Huang, Huanwei, Xuyan W et al (2015) Cleavage of GSDMD by inflammatory caspases determines pyroptotic cell death. Nature

26. Karmakar M, Minns M, Greenberg EN, Diaz-Aponte J, Pearlman E (2020) N-GSDMD trafficking to neutrophil organelles facilitates IL-1β release independently of plasma membrane pores and pyroptosis. Nat Commun. ;11(1)
27. Xixi Z, Haibing Z (2018) Chemotherapy drugs induce pyroptosis through caspase-3-dependent cleavage of GSDME. Sci China(Life Sciences) 61(06):129–130
28. Hu L, Chen M, Chen X, Zhao C, Dai H (2020) Chemotherapy-induced pyroptosis is mediated by BAK/BAX-caspase-3-GSDME pathway and inhibited by 2-bromopalmitate. Cell Death Dis. ;11(4)
29. Zhang Z, Zhang Y, Xia S, Kong Q, Lieberman J (2020) Gasdermin E suppresses tumour growth by activating anti-tumour immunity. Nature 579:7799
30. Gao W, Wang X, Zhou Y, Wang X, Yu Y (2022) Autophagy,ferroptosis,pyroptosis,and necroptosis in tumor immunotherapy. Signal Transduct Target Therapy 7(7):26
31. Hu H, Tian M, Ding C, Yu S (2019) The C/EBP Homologous Protein (CHOP) Transcription Factor Functions in Endoplasmic Reticulum Stress-Induced Apoptosis and Microbial Infection. Front Immunol. ;9
32. Faries MB, Bedrosian I, Xu S, Koski G, Czerniecki BJ (2001) Calcium signaling inhibits interleukin-12 production and activates CD83(+) dendritic cells that induce Th2 cell development. Blood 98(8):2489
33. Aggarwal BB, Gupta SC, Kim JH (2012) Historical perspectives on tumor necrosis factor and its superfamily: 25 years later, a golden journey. Blood 119(3):651–665
34. Zhang Z, Zou J, Shi Z, Zhang B, Gewirtz AT (2020) IL-22-induced cell extrusion and IL-18-induced cell death prevent and cure rotavirus infection. Sci Immunol. ;5(52)
35. Iwata TN, Ishii C, Ishida S, Ogitani Y, Wada T, Agatsuma T (2018) A HER2-targeting antibody-drug conjugate, trastuzumab deruxtecan (DS-8201a), enhances antitumor immunity in a mouse model. Molecular Cancer Therapeutics. :molcanther.0749.2017
36. Niu X, Chen L, Li Y, Hu Z, He F (2022) Ferroptosis, necroptosis, and pyroptosis in the tumor microenvironment: Perspectives for immunotherapy of SCLC. Sem Cancer Biol 86(Pt 3):273–285
37. W MWM, L X, J. H SS (2022) B. L, Pyroptosis Remodeling Tumor Microenvironment to Enhance Pancreatic Cancer Immunotherapy Driven by Membrane Anchoring Photosensitizer. Adv Sci
38. L NLWAHSV, C P, W H (2023) MP. B. An anti-mesothelin targeting antibody drug conjugate induces pyroptosis and ignites antitumor immunity in mouse models of cancer. J Immunother Cancer. ;11(3)
39. Wang Q, Wang Y, Ding J, Wang C, Zhou X, Gao W et al (2020) A bioorthogonal system reveals antitumour immune function of pyroptosis. Nature 579(7799):421–426
40. Li D, Xie K, Wolff R, Abbruzzese JL (2004) Pancreatic cancer. Lancet 363(9414):1049–1057

Figures

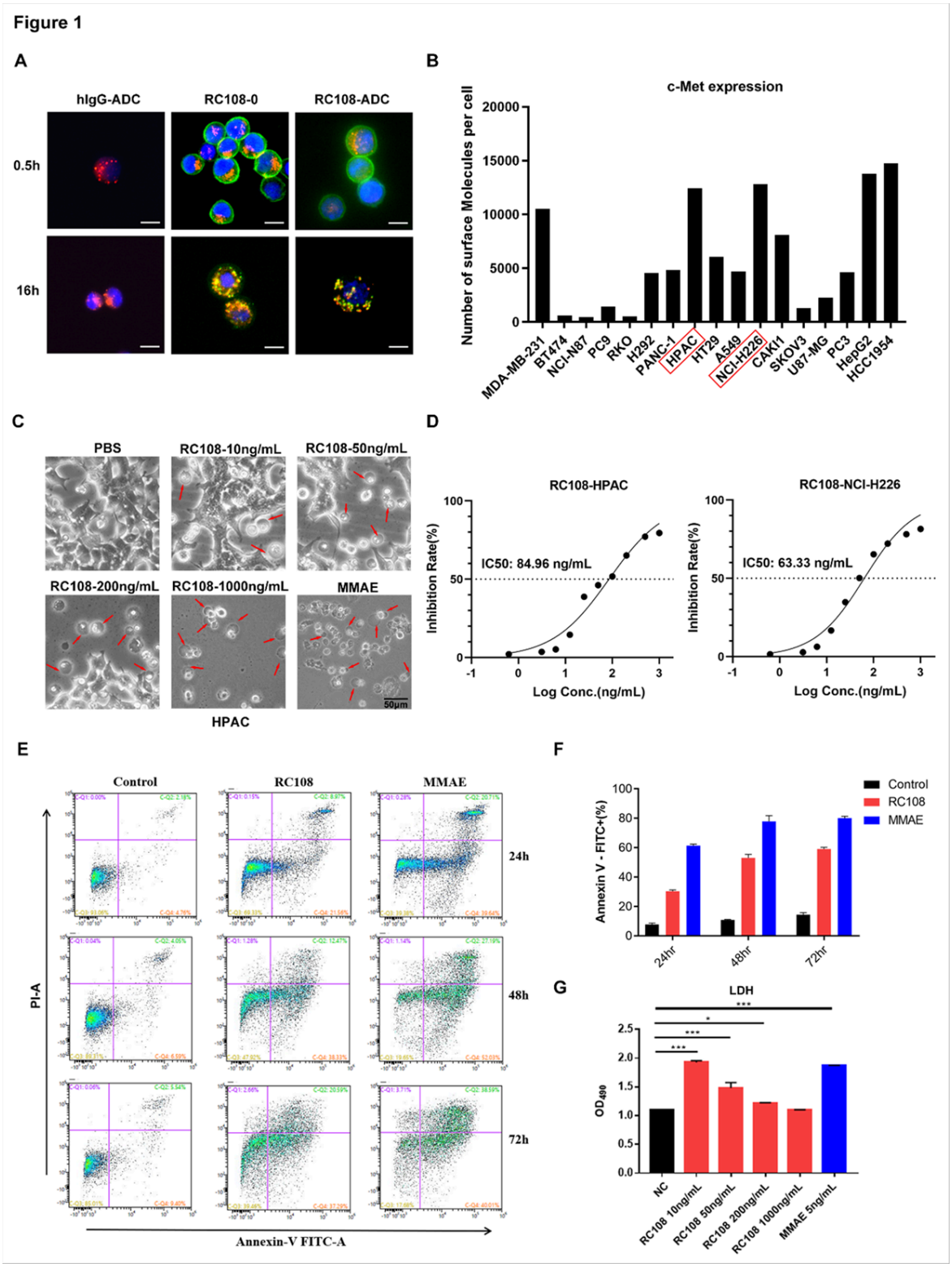


Figure 1

RC108 and MMAE induce pyroptosis. A, MKN-45 cells were processed by hIgG-ADC, RC108-0, and RC108-ADC. Fluorescent signals were tracked and labeled at 0.5h and 16h respectively. hIgG-ADC, Homologous antibody of RC108 coupled with MMAE; RC108-0, c-Met monoclonal antibody uncoupled with MMAE; RC108-ADC, c-Met monoclonal antibody coupled with MMAE. **B,** Flow cytometry analysis of c-Met protein expression levels in various cell lines. **C,**Representative figure of HPAC pyroptosis

phenotype induced by RC108 or MMAE at 48h. **D,** The IC50 value of RC108 in HPAC and NCI-H226 cells at 72 hours was detected by the cck-8 assay. **E,** Annexin-V and PI double staining was used to detect cell death induced by RC108 and MMAE in HPAC cells at different time points. **F,** The statistical chart of the Figure E. **G,** Various concentrations of RC108 and MMAE induced LDH release levels in HPAC cells at 72 hours. Data analyses were performed by GraphPad Prims 8, ANOVA. Error bars, means ± SD (n = 3). * P < 0.05; ** P < 0.01; *** P < 0.001.

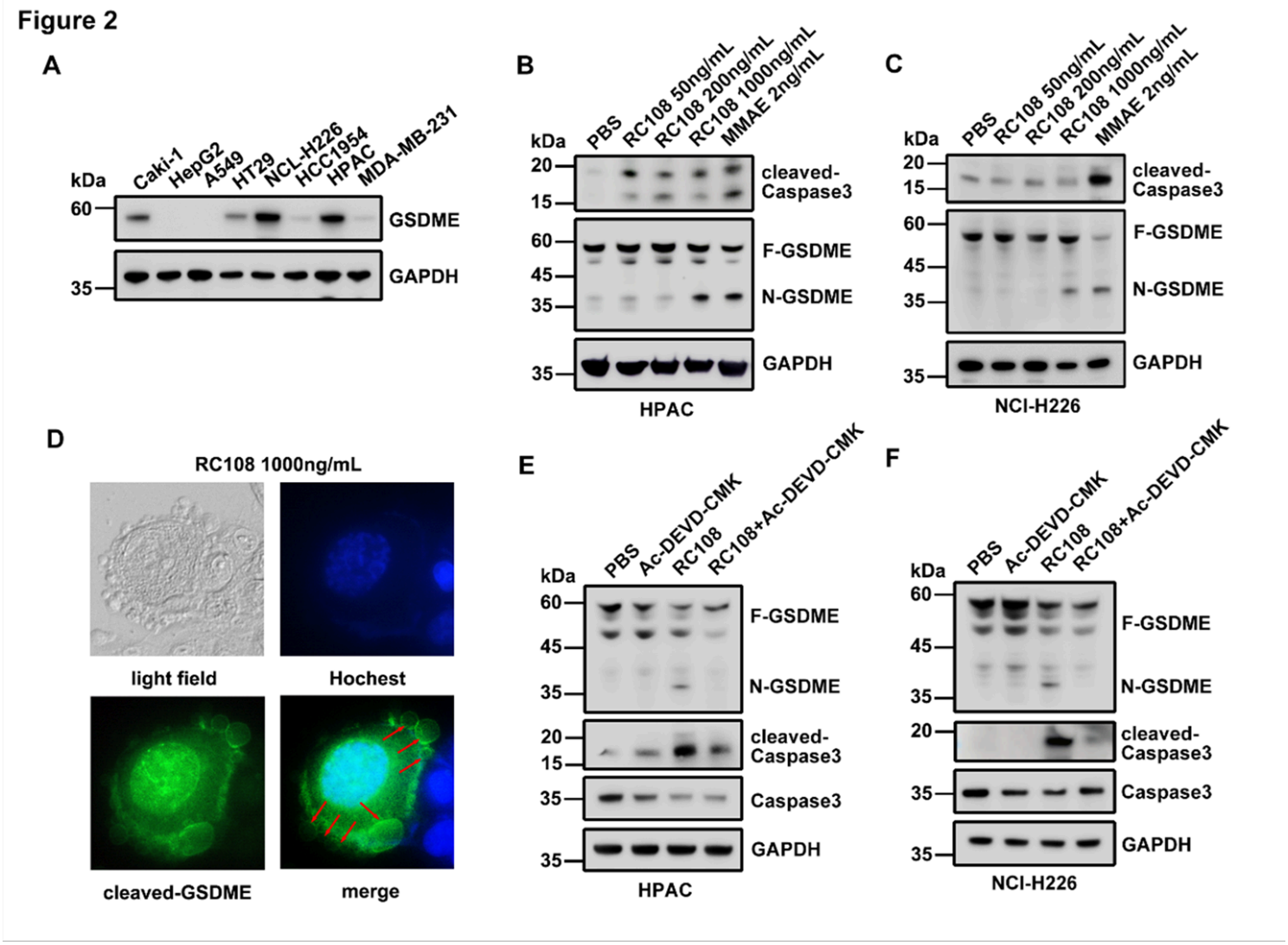


Figure 2

RC108 mediates pyroptosis by Caspase3-GSDME. A, Western blot analysis of GSDME expression in cell lines. **B, C,** Western blot analysis of cleaved-Caspase3 and GSDME in HPAC and NCI-H226 cells activated by RC108 and MMAE. **D,** Immunofluorescence staining of cleaved GSDME location induced by RC108. **E, F,** Western blot analysis of cleaved-Caspase3 and GSDME in HPAC and NCI-H226 cells activated by 1000ng/mL RC108 and/or 20μM Ac-DEVD-CMK for 48h.

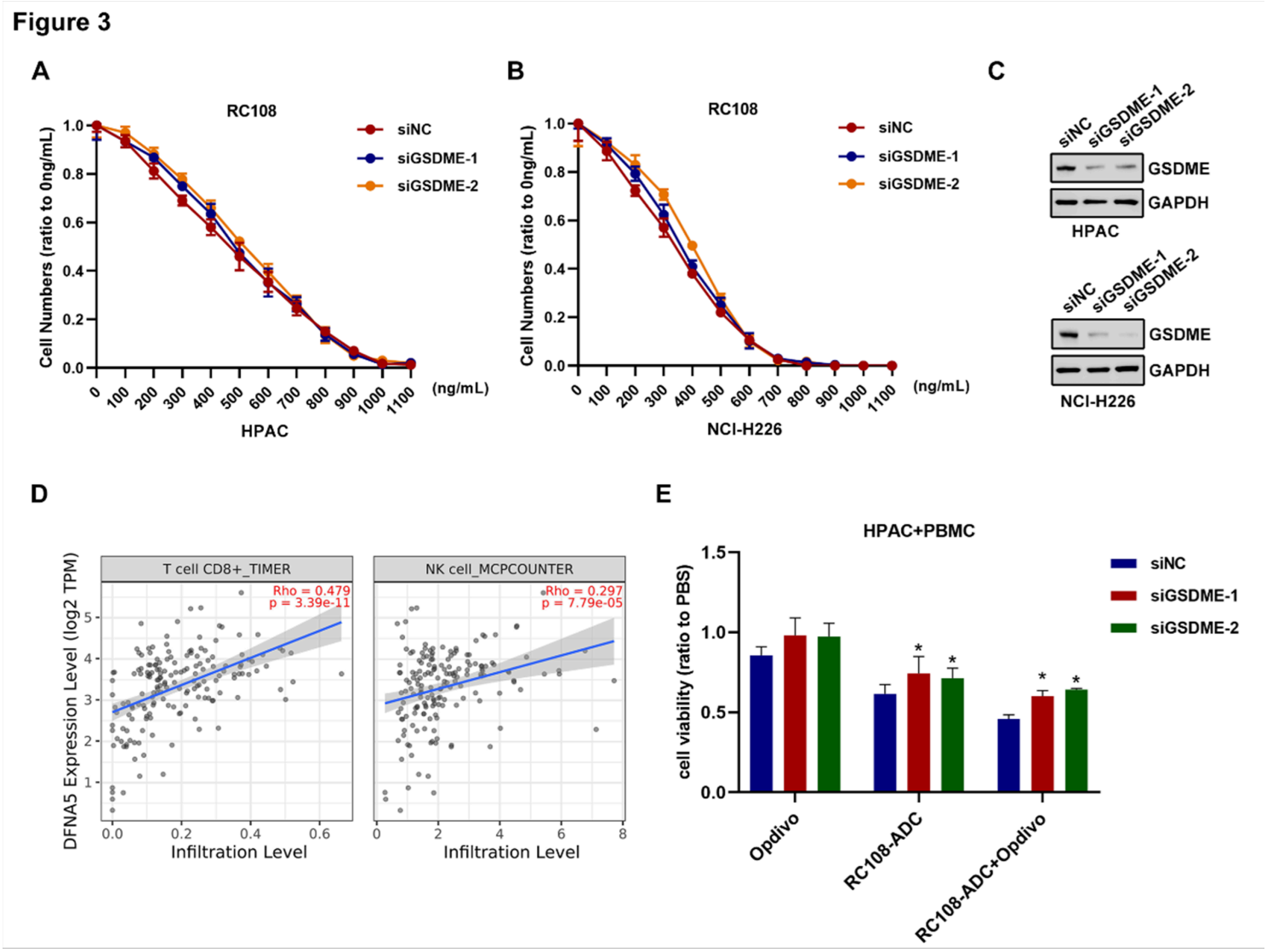


Figure 3

Pyroptosis regulates combination of RC108 and Opdivo to inhibit tumor cell growth *in vitro*. A, B, GSDME silenced HPAC and NCI-H226 cells were treated with RC108 at various concentrations, and subsequently cell counting was performed. The ordinate represents the normalized results of all groups compared with the 0ng/mL RC108 group. **C,** Western blot analysis of GSDME expression levels in HPAC and NCI-H226 cells of GSDME knockdown. **D,** Correlation analysis between DFNA5 (GSDME gene name) and $CD8^+$ T cells or NK cells infiltration in tumors obtained from TIMER2.0 website. **E,** With GSDME silencing, the effect of RC108 combined with Opdivo on hPBMC killing HPAC cell. The cck-8 assay was used to detect the viability of adherent tumor cells.

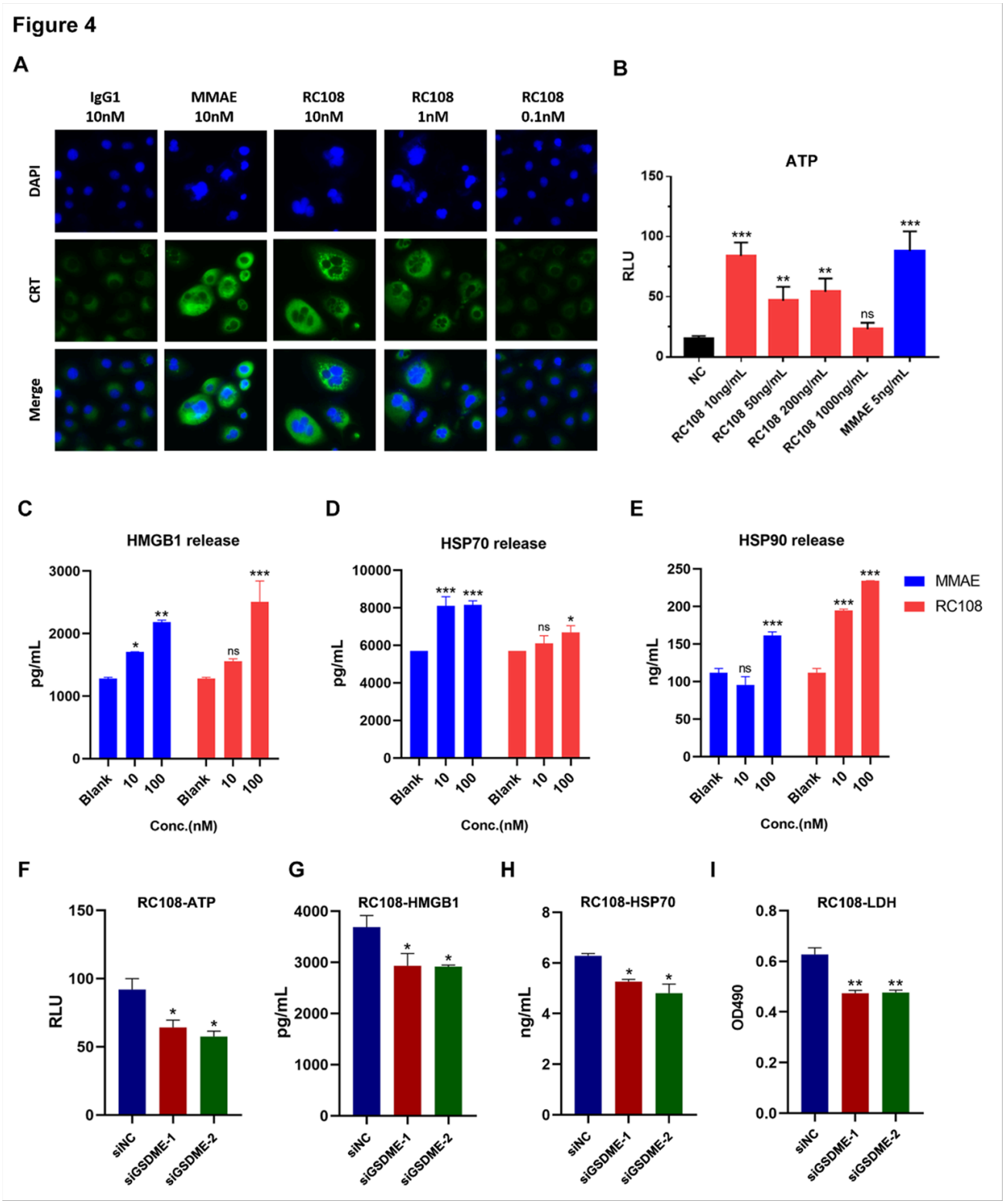


Figure 4

The attenuation of pyroptosis reverses the release of DAMPs induced by RC108. A, Immunofluorescence data of calreticulin (CRT) protein expression activated by RC108 at various concentrations or MMAE. **B,** Statistics of ATP levels in cell supernatants promoted by RC108 at various concentrations or MMAE. **C-E,** ELISA results of HMGB1, HSP70 and HSP90 induced by RC108 at various concentrations or MMAE. **F-I,** With GSDME knockdown for 24h, ATP, HMGB1, HSP70 and LDH release

regulated by 500ng/mL RC108 were detected using specific-ELISA kit. The drug treatment time for all figures was 48h. Data analyses were performed by GraphPad Prims 8, two-tailed t-test. Error bars, means ± SD (n = 3). * $P < 0.05$; ** $P < 0.01$; *** $P < 0.001$.

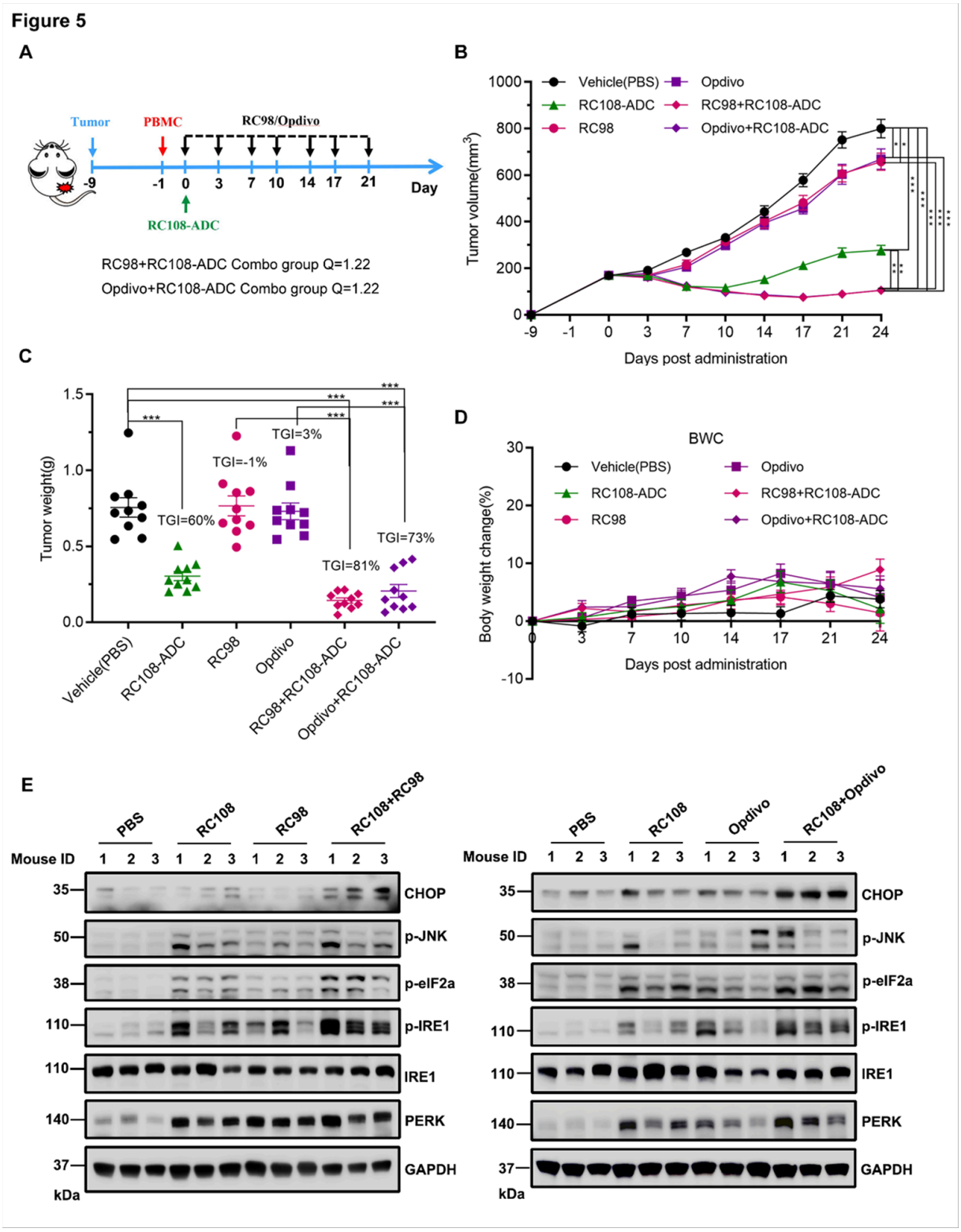


Figure 5

RC108 combined with PD-1/PD-L1 blockade exerts synergistic tumor inhibition effect. A, The flow chart of *in vivo* study of combination drugs. The injection time and frequency for all groups were shown in the figure. The Q value represented the synergistic effect of the combination group compared with the single drug group according to the specific calculation formula. **B,** At regular intervals, vernier calipers were used to measure the tumor volume of tumor-bearing mice (n=10). **C.** At the endpoint (Day24), all mice were euthanized and tumors were removed. Tumor weight was measured and compared with vehicle group to obtain tumor growth inhibition (TGI). **D,** At regular intervals, the weight of mice was measured to calculate the weight change rate. E, Western blot analysis for ER-Stress signal from 3 individuals from each group. Data analyses were performed by GraphPad Prims 8, ANOVA. Error bars, means ± SD. * $P < 0.05$; ** $P < 0.01$; ***$P < 0.001$.

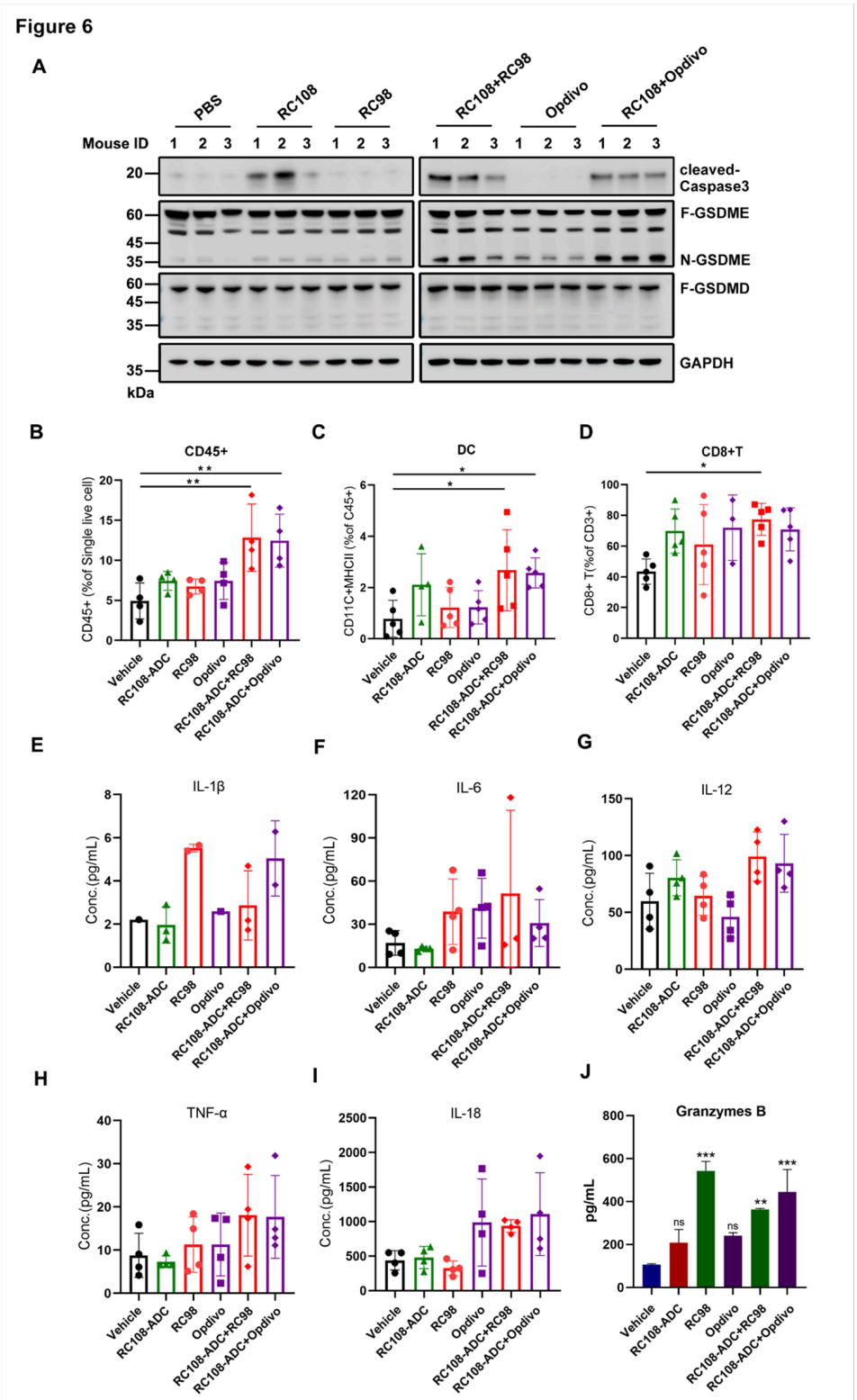


Figure 6

RC108 alone or in combination with ICIs induces tumor pyroptosis and ICD. A, Western blot analysis for Caspase, GSDME and GSDMD from 3 individuals from each group. **B-D,** The infiltration of $CD45^+$, DC, $CD8^+$ T cells in all xenografts was quantified by flow cytometry. **E-J,** CBA quantitative analysis of DC and $CD8^+$ T cells related cytokines in serum of all groups. Data analyses were performed by GraphPad Prims 8, ANOVA. Error bars, means ± SD. * $P < 0.05$; ** $P < 0.01$; *** $P < 0.001$.

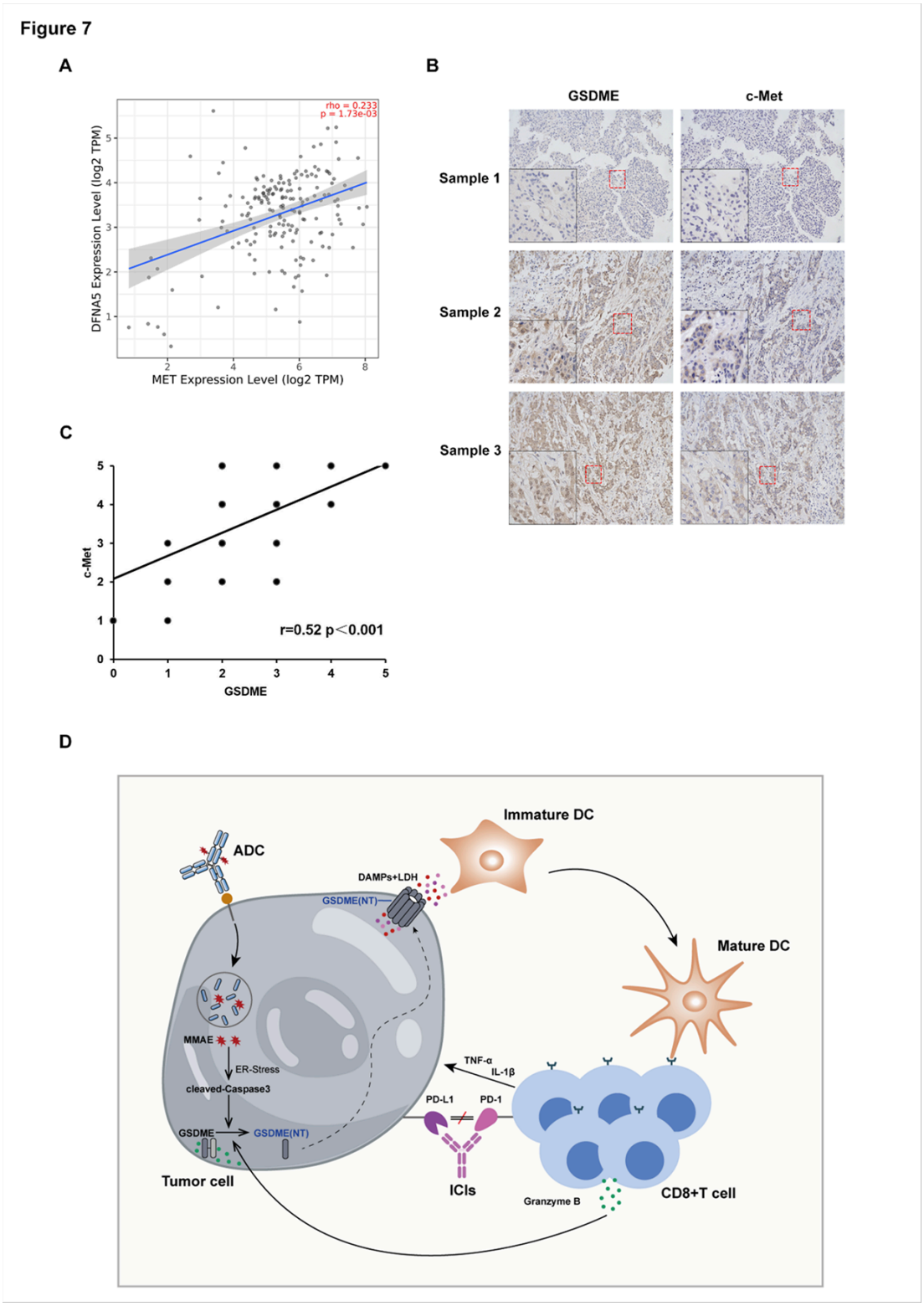


Figure 7

GSDME is a suitable screening marker for the combination therapy of ADC targeting c-Met and PD-1/PD-L1 blockade in pancreatic cancer. A, The correlation between GSDME gene and c-met gene expression in pancreatic cancer was analyzed by TIMER2.0 software. **B,** Representative results of immunohistochemical staining of GSDME and c-Met on tissue microarrays containing tumor samples from 71 patients with pancreatic cancer. Two consecutive sections of each sample were evaluated by

GSDME and c-Met antibodies respectively. The red dotted line marked the area corresponding to the high magnification image. **C,** Statistical analysis of the Pearson correlation between the immunohistochemical staining score of GSDME expression and c-Met expression. **D,** Schematic diagram of the synergistic tumor suppressive effect of RC108 combined with ICIs regulated by pyroptosis. The intracellular payload MMAE released by ADC activated Caspase3-GSDME axis. The release of DAMPs induced by activated GSDME ignited immune response. ICIs assisted ADC in inhibiting tumor growth by reversing exhausted $CD8^+$ T cells.

Supplementary Files

This is a list of supplementary files associated with this preprint. Click to download.

- SupplementaryInformation.docx